Mechanical behavior and constitutive model of sustainable concrete: seawater and sea-sand recycled aggregate concrete

Wanhui Feng[1], Yunchao Tang[1,2,3*], Yongmin Yang[1], Ye Cheng[1], Jianhui Qiu[1], Hexin Zhang[4], Haytham F. Isleem[5], Bassam A. Tayeh[6], Abdoullah Namdar[7]

[1] Guangdong Lingnan Township Green Building Industrialization Engineering Technology Research Center, Zhongkai University of Agriculture and Engineering, Guangzhou 510225, China

[2] Key Laboratory of Disaster Prevention and Structural Safety of Ministry of Education, School of Civil Engineering and Architecture, Guangxi University, Nanning 530004, China

[3] Guangxi Key Laboratory of Disaster Prevention and Engineering Safety, Guangxi University, Nanning 530004, China

[4] School of Computing, Engineering and the Built Environment, Edinburgh Napier University, 10 Colinton Road, Edinburgh, Scotland, UK, EH10 5DT

[5] Department of Construction Management, Qujing Normal University, Qujing 655011, Yunnan, China

[6] Civil Engineering Department, Faculty of Engineering, Islamic University of Gaza, P.O. Box 108, Gaza Strip, Palestine

[7] School of Civil Engineering, Iran University of Science and Technology (IUST), Narmak, Tehran, Iran

* Corresponding author

Email: joshua0115@gxu.edu.cn (Yunchao Tang)

Abstract: Resources such as fresh water and river sand have become scarce in some areas around the world because of the considerable increase in infrastructural construction. To overcome this issue, the utilization of recycled aggregates (RAs) in concrete is considered a sustainable construction method. Due to the growing scarcity of river sand and fresh water, this study explores the mechanical properties of recycled aggregate concrete (RAC) incorporated with seawater (SW) and sea sand (SS), referred to as SWSSRAC. To this end, a total of 18 mix ratios were designed to analyze the effects of different water-to-cement ratios, curing ages, and RA replacement rates on the mechanical properties of the SWSSRAC. The results suggest that the fluidity of SWSSRAC is slightly worse than that of RAC; further, the effect of the RA replacement rate on the fluidity of concrete is greater than that of SW and SS. The stress–strain relationship reveals that the deformation capacity of SWSSRAC at curing ages of 28 and 180 days show a higher improvement attributed to SW and SS for RAC compared to that for natural aggregate concrete (NAC). In addition, using SW and SS improves the compressive strength and elastic modulus of RAC, particularly after curing for 28 days; the enhancement effect of SW and SS on the mechanical properties of RAC is higher than that of NAC. Although the unloading segments in the stress–strain relationship of SWSSRAC are different from those of RAC at the 28-day curing age, it is necessary to use constitutive models of RAC for SWSSRAC considering long-term use. According to the findings of this study, SW and SS are more suited for RAC than NAC.

Keywords: Recycled aggregate concrete; Seawater; Sea sand; Compressive behavior; Stress–strain relationship

1. Introduction

Concrete is the primary material used in construction and infrastructure, and its consumption is increasing with the growth in the building industry [1–3]. Many structures are being demolished as cities continue to grow, which results in massive volumes of construction and demolition (C&D) waste [4]. In China, approximately 5% of C&D debris is recycled [5]. Some researchers [6–9] found that recycled aggregate (RA) produced by C&D can be utilized in fresh concrete to reduce the environmental impact, which is known as recycled aggregate concrete (RAC). Furthermore, the consumption of fresh water (FW) and river sand (RS) has skyrocketed, which results in a scarcity of natural resources and negative effects on the environment. Significant efforts have been made to identify novel and recycled waste materials to compensate for the scarcity of natural fine aggregates. Meanwhile, water covers approximately 71% of the Earth's surface area, where seawater (SW) accounts for 97% of the total water, and this implies FW and RS resources are limited [10]. The use of sea sand (SS) as a raw material for reinforced concrete construction has been restricted in numerous countries because of chloride ions in the SS which corrode the reinforcement. Recently, Teng et al. [11] presented fiber-reinforced polymer (FRP) composites as a viable alternative to steel bars for SS concrete in offshore engineering because of their excellent corrosion resistance. Therefore, SS and SW can be utilized in RAC to further promote sustainable construction materials. Fig. 1 depicts the recycling process of ecologically friendly buildings.

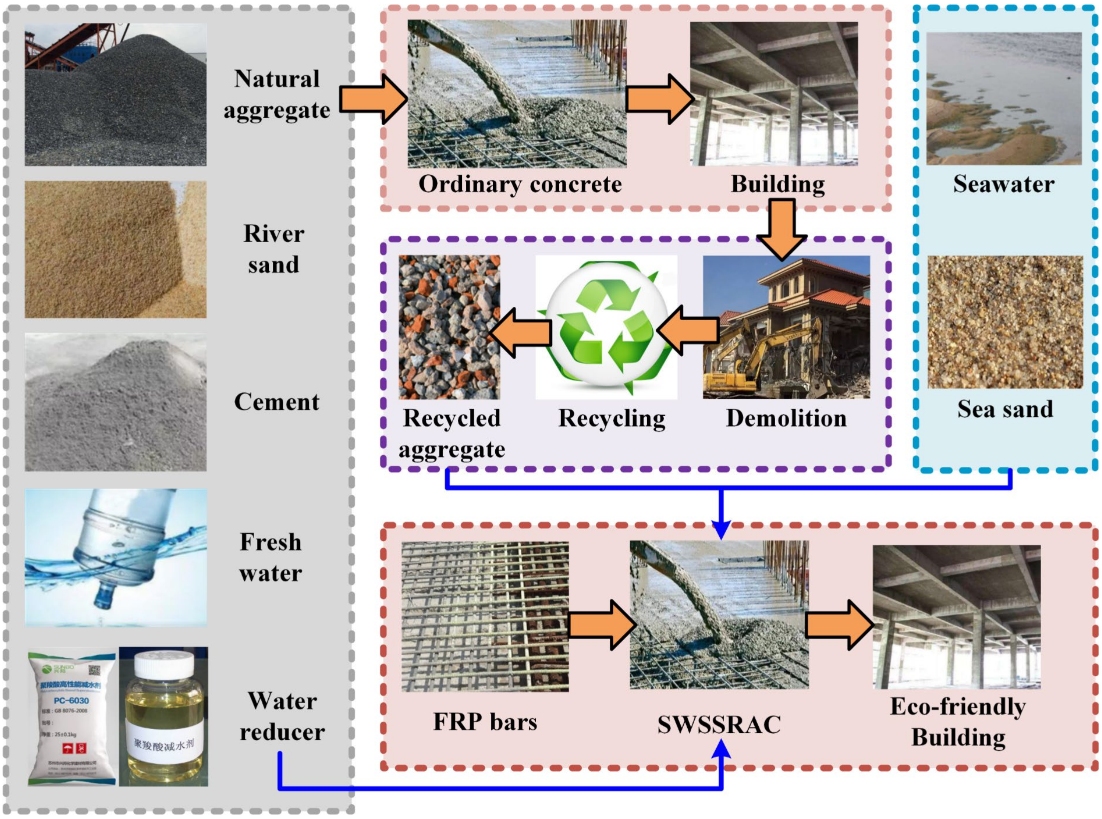

Fig. 1. Recycling process of ecologically friendly buildings

In addition to the negative effects of SW on the durability of concrete and steel reinforcement, sulfate ions in SW accelerate the production of gypsum and ettringite which leads to concrete cracking [12]. Hence, the salinity and chemical composition of SW have significant effects on the pore structure of concrete incorporating SW. The porosity of concrete also increases with an increase in the salinity of SW [13]. In addition, Islam et al. [14] found that the higher early aged strength of SW concrete was attributed to the reaction between the salts in SW and the cement paste to generate hydrates; this led to the filling of the micropores and enhancement of the compressive strength of concrete. However, the long-term strength decreases slightly compared to ordinary concrete because of the leaching of soft hydration products from the concrete. Eziefula et al. [15] highlighted that the compressive strength of concrete decreased because of the crystallization of salt (sodium chloride) in SW at later curing ages.

SS is similar to SW, and many ions have negative effects on concrete and steel bars. In addition, compared with RS, SS contains many impurities such as shells. Yang et al. [16] proposed that shells had no significant effect on the strength of concrete. However, the working performance of the concrete is weakened when the shell content is high. In other words, the properties of SS concrete can be enhanced if the seashells are removed. Limeira et al. [17] proved that the compressive strength of SS concrete (25−50% SS-replaced RS) could be enhanced by removing impurities. Furthermore, the surface of SS is more rough than that of RS because of repeated scouring by waves, which results in higher bonding properties of the interface transition zone (ITZ) [18]. Some researchers [19,20] concluded that partially replacing RS with SS could improve the gradation of fine aggregates and enhance the strength of concrete.

The mechanical properties exhibit remarkable changes when SS and SW are used together in concrete. However, there are few studies on the utilization of SW and SS in RAC. The RAC has different ITZs compared to ordinary concrete (natural aggregate concrete [NAC]) because of the adhered mortar on the surface of RAs [21,22] and many microcracks [23]. Therefore, Etxeberria et al. [24] and Alexandriou et al. [25] found that 75% and 100% RA replacement ratios resulted in 37% and 25% reductions in compressive strength, respectively. Based on these conclusions, one of the most important factors affecting the mechanical characteristics of RAC is the amount of RA used. Further, it can be inferred that the replacement rate of RA affects the mechanical properties of concrete containing SW and SS. It is necessary to conduct a series of experiments on RAC that incorporates SS and SW (SWSSRAC) to understand its mechanical properties.

This study aims to analyze the effect of using SW and SS as aggregates on the properties of RAC, that is, to determine the compressive behaviors and constitutive models of SWSSRAC with various RA replacement rates. In addition, the RA replacement rate (0%, 50%, and 100%), concrete strength grade (30 MPa, 40 MPa, and 50 MPa), and curing age (28, 60, and 180 days) were used as the research parameters. Further, this study provides a reference for engineering applications, and the constitutive model can help perform numerical analysis in the future.

The remainder of this paper is organized as follows: Section 2 describes the physical properties of the raw materials and the preparation of SWSSRAC. Section 3 illustrates the experimental arrangements, which includes equipment and procedures. Section 4 presents the experimental results of SWSSRAC compared with those of NAC. Further, some existing constitutive models are compared with the experimental stress–strain curves of the SWSSRAC in Section 5. The conclusions and recommendations are presented in Section 6.

2. Raw materials, mix proportions, and specimen preparation

2.1. Raw materials

Artificial SW was used based on requirements in the ASTM D1141 [26]; the chemical composition of the artificial SW is listed in Table 1. The chlorinity of the SW substitute is approximately 1.938%. In addition, ordinary Portland cement with a nominal compressive strength of 42.5 MPa (P.O. 42.5R) is used, and the cement parameters are summarized in Table 2. There were two types of fine aggregates (SS and RS) were used. In the Nansha District of Guangzhou City, SS with a chlorinity of 0.082%, maximum particle size of 2.40 mm, fineness modulus of 1.58, and apparent density of 2561 kg/m^3 was prepared. RS with a maximum particle size of 2.40 mm, fineness modulus of 2.36, and apparent density of 2586 kg/m^3 was also prepared. For coarse aggregates, RA and NA with particle sizes of 4.75−26.50 mm and continuous grading were utilized. The RAs were produced from abandoned structures in Shenzhen City. Besides, RAs with particle sizes less than 4.75 mm and greater than 26.5 mm were eliminated to minimize the influence of RAs and NAs attributed to particle size. The physical properties of coarse aggregates are listed in Table 3. Grading curves of the fine and coarse aggregates are shown in Fig. 2. Based on the requirements in the JGJ 52 [27], the grading curves of RS was satisfied with Grade III, but the averaged particle size of SS was smaller than that of RS. Besides, RA and NA were both consistent with the requirements in the JGJ 52 [27]. A brown liquid naphthalene superplasticizer with a solid content of 29.7% and water reduction rate of 40% was adopted to obtain a good working performance.

Table 1 Chemical composition of artificial SW

Compound	NaCl	Na_2SO_4	KCl	$CaCl_2$	$MgCl_2{\cdot}6H_2O$
Concentration (g/L)	24.5	4.1	0.7	1.2	11.1

Table 2 Typical properties of cement

Chemical composition (%)		Loss on ignition	Standard consistency	Setting time (min)		Flexural strength (MPa)		Compressive Strength (MPa)	
SO_3	MgO	(%)	(%)	Initial	Final	3 d	28 d	3 d	28 d
1.85	1.95	2.10	27.50	155	220	5.3	9.4	27.5	50.3

Table 3 Physical properties of coarse aggregate

Material Type	Apparent density (kg/m^3)	Water absorption (%)	Sediment content (%)	Elongated particles (%)	Crushing index
RA	2481	4.39	0.4	8.9	10.8
NA	2657	1.24	0.2	9.3	8.3

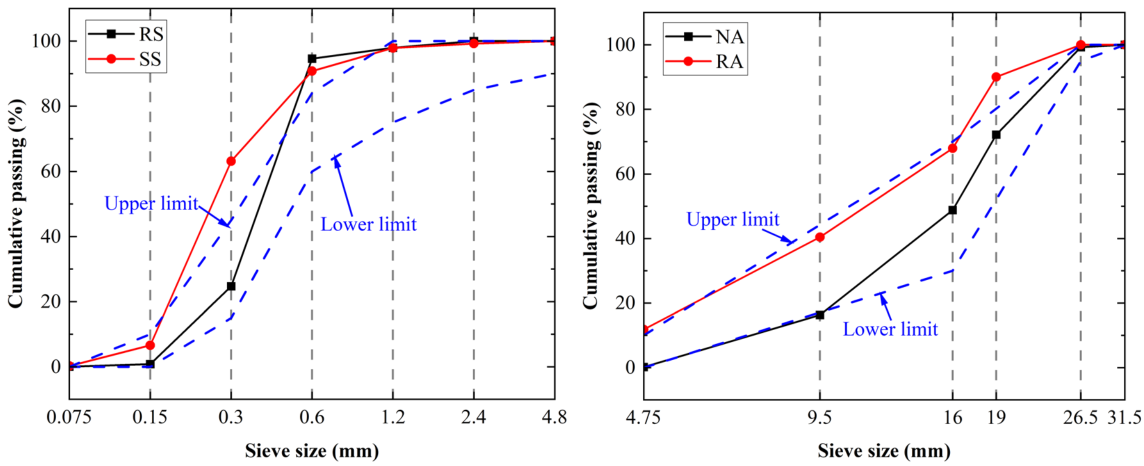

(a) (b)

Fig. 2. Grading curves of (a) fine aggregate and (b) coarse aggregate

2.2. Design of mix proportions

Three design grades of concrete strength (C30, C40, and C50) were designed based on Chinese standard JGJ55 [28] to better understand the effects of SS, SW, and RA on the mechanical properties of SWSSRAC. The water-to-binder ratios of the C30, C40 and C50 strength grades were 0.51, 0.44, and 0.37, respectively. Also, additional water was added to the mix proportions based on the difference in the absorption rate between NA and RA measured in Table 3. SS and RA were added to fresh concrete by replacing equal volumes of RS and NA, respectively. There is no need to study the partial replacement rate of SS in concrete mixes incorporating SW because SS has high chlorinity and can easily exceed the allowable value of chloride ions in ordinary concrete structures. Hence, concrete mixes with SW and SS should be used with FRP bars in building construction. Here, 100% of RS was replaced with SS in the concrete mixes. All mix proportions are listed in Table 4, where “30,” “40,” and “50” represent the design grade of strength and “-50” and “-100” represent the RA replacement rate. For example, "SWSSNAC30" represents the NAC with the strength grade of C30 incorporating SW and SS; "RAC40-50" represents the RAC with the strength grade of C40 incorporating FW and RS and a RA replacement rate of 50%.

Table 4 Summary of mix proportions

ID	Raw material (kg/m^3)							
	FW	SW	Cement	RS	SS	NA	RA	Superplasticizer
NAC30	200	0	390	635	0	1180	0	0
NAC40	195	0	443	576	0	1171	0	0
NAC50	167	0	452	649	0	1138	0	3.5
SWSSNAC30	0	200	390	0	629	1180	0	0
SWSSNAC40	0	195	443	0	570	1171	0	0
SWSSNAC50	0	167	452	0	643	1138	0	3.5
RAC30-50	217	0	390	635	0	590	551	0
RAC40-50	212	0	443	576	0	586	547	0
RAC50-50	184	0	452	649	0	569	531	3.5
SWSSRAC30-50	0	217	390	0	629	590	551	0
SWSSRAC40-50	0	212	443	0	570	586	547	0
SWSSRAC50-50	0	184	452	0	643	569	531	3.5
RAC30-100	235	0	390	635	0	0	1102	0
RAC40-100	229	0	443	576	0	0	1093	0
RAC50-100	200	0	452	649	0	0	1063	3.5
SWSSRAC30-100	0	235	390	0	629	0	1102	0
SWSSRAC40-100	0	229	443	0	570	0	1093	0
SWSSRAC50-100	0	200	452	0	643	0	1063	3.5

2.3. Specimen preparation

Raw materials were measured according to the mix proportion and then the coarse and fine aggregates were poured into a concrete mixer for 60 seconds under dry conditions. Subsequently, half of the mixing water was added to the mixer and mixed for 60 s. Finally, the cement and remaining water were poured into the mixer and mixed for 120 s. After testing the working performance, fresh concrete was cast into molds and vibrated using a vibrator. Based on the requirements in the Chinese standard GB/T 50081 [29], all specimens were demolded after 24 hours and cured under standard conditions (room temperature 20 ± 2 °C, relative humidity higher than 95%) until reaching the target curing day (28, 60, or 180 days). Photographs of the raw materials and specimen preparations are shown in Fig. 3.

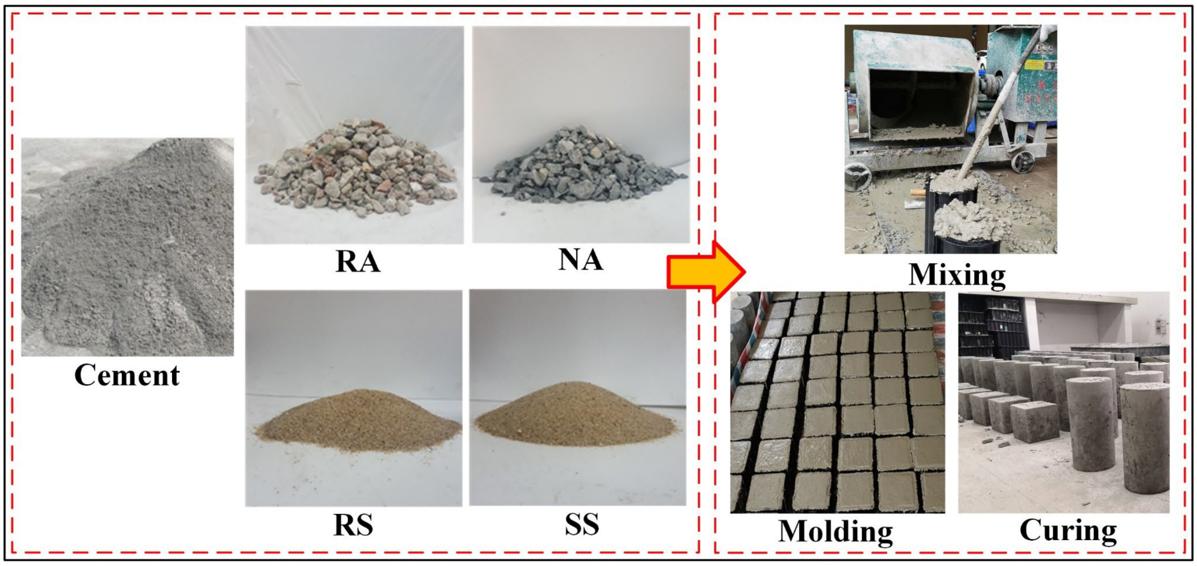

Fig. 3. Photos of raw materials and specimen preparation

3. Experimental methods

3.1. Cubic compression test

A universal compression machine was employed to measure the cubic compression strength of the specimens based on the requirements of the Chinese standard GB/T 50081 [29]. The loading rate was set at 0.5 MPa/s. Further, the edge length of all cubes was 150 mm, and the cubic compressive strength was averaged from three cubes of each mix proportion. A photograph of the cubic compression test setup is shown in Fig. 4.

Fig. 4. Photo of the cubic compression test

3.2. Uniaxial compression test

According to the requirements of ASTM standards C39 [30] and C469 [31], cylinders with a diameter of 150 mm and height of 300 mm were tested using a uniaxial compression machine to measure the uniaxial compressive strength, elastic modulus, Poisson's ratio, and stress–strain relationship. Fig. 5 shows that both ends of the cylinder were first levelled with a gypsum-leveling layer. Two longitudinal strain gauges with lengths of 100 mm and two circumferential strain gauges with lengths of 80 mm were applied on the middle surface of each cylinder. Lubricating oil was used to reduce the friction coefficient between the ends of the specimen and loading platform before the compression started. Finally, two 120-mm-length linear variable differential transformers (LVDTs) were installed to capture the longitudinal displacement history of the middle height of each cylinder because the strain gauges easily failed in the plastic phase during compression. The loading rate was set to 0.18 mm/min, and the end of each test was set to 10% of the maximum load at the unloading stage of each specimen. A strain acquisition system (JM3841, China) was used to record all data, with the sampling rate set to 1 Hz.

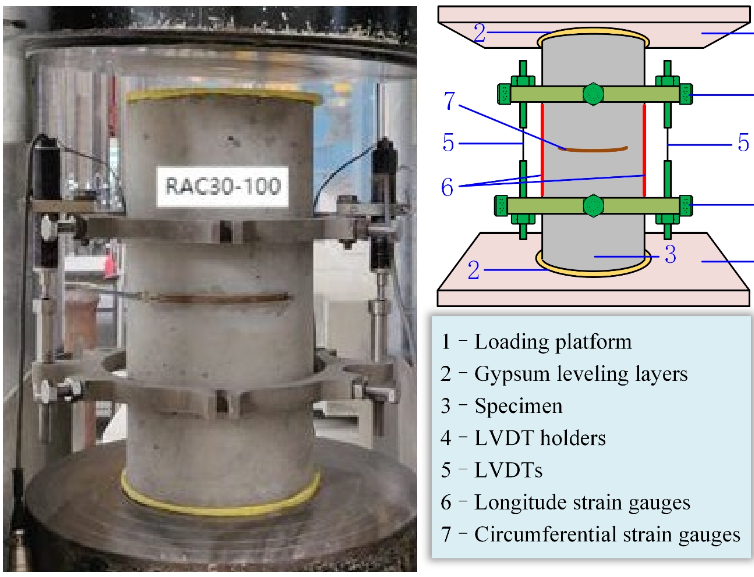

Fig. 5. Photograph and sketch of the uniaxial compression test

4. Experimental results

4.1. Working performance

The results showed that the slump decreased obviously with an increasing RA replacement rate and with a decreasing of water-to-cement ratio, as shown in Fig. 6. Compared with NA, RA reduces the working performance of fresh concrete because of its higher porosity; the low water-to-binder ratio obviously weakens the slump of concrete. In addition, the fluidities of SWSSNAC and SWSSRAC were lower than those of NAC and RAC. Compared with NAC30, NAC40, and NAC50, the slumps of SWSSNAC30, SWSSNAC40, and SWSSNAC50 were reduced by approximately 20%, which is consistent with the results of Liu et al. [32] (22%) and Ting et al. [33] (26%). One reason is that the fineness modulus of SS is smaller than that of RS; the specific surface area is larger than that of RS, and this leads to a larger water absorption rate of SS [18]. Further, many ions in the SW react with the cement. Hence, the actual water-to-binder ratio was decreased by incorporating the SS. However, the negative effects of SW and SS on slump were reduced with an increase in the RA replacement rate. For example, the slump of SWSSRAC with a 100% RA replacement rate only decreased by approximately 15% compared with RAC. This is because water was absorbed which reduced the actual water-to-cement ratio and delayed the hydration reaction speed between SW and cement. Similarly, the influence of SS and SW on the slump decreases because the water-to-cement ratio decreases from 0.51 to 0.37 [32]. Besides, for the high-strength concrete, taking the specimens with the water-to-cement ratio was 0.37 as the examples, when the RA replacement rates increased to 50% and 100%, the slumps decreased 35 mm and 25 mm, respectively. However, if SW and SS were added into NAC50, RAC50-50, and RAC50-100, the slumps were only reduced 25 mm, 10 mm and 10 mm, which indicated that the effects of SW and SS on the working performance of high-strength concrete was not obvious.

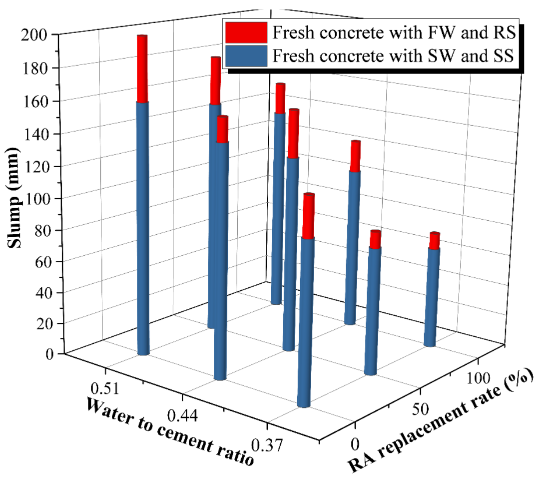

Fig. 6. Experimental results of working performance

4.2. Cubic compressive strength

The experimental results of the cubic compression tests are summarized in Table 5. In the curing age period of 28–180 days, the growth rate of RAC in the later stage is not as large as that of NAC. In addition, SW and SS have a negative effect on the growth of later-age strength; however, the greater the water-to-cement ratio, the more significant the influence of SW and SS on the strength growth rate. This is similar to the conclusion of the working performance. As shown in Fig. 7, SW and SS can improve the 28-day strength of concrete in general, particularly for RAC with a 100% RA replacement rate. The 28-day strength of SWSSRAC30-100 was approximately 20% higher than that of RAC30-100. This implies that, although the strength of RAC is lower than that of NAC under the same water-to-cement ratio, SW and SS can compensate for the strength loss caused by the defects of RAs like the microcracks in the old mortar in the RAC. In addition, SW and SS enhance the strength of RAC at 180 days because the long-term properties of concrete incorporating SW and SS are key factors. Therefore, hydrates produced by the early hydration reaction between ions in SW, SS, and cement are harmful to NAC, whereas for RAC, the hydrates fill the microcracks of RAs and promote the strength. In other words, SS, SW, and RA can be used together in concrete materials.

Table 5 Experimental results of cubic compression test

ID	Strength (MPa)		Growth rate (%)	ID	Strength (MPa)		Growth rate (%)
	28 d	180 d			28 d	180 d	
NAC30	38.1±1.3	43.8±1.2	14.9	SWSSNAC30	40.2±2.5	42.2±1.7	5.1
NAC40	50.1±3.9	60.0±2.0	19.7	SWSSNAC40	45.4±2.7	51.9±3.5	14.2
NAC50	56.3±3.2	63.1±0.9	12.0	SWSSNAC50	50.4±2.9	61.4±1.8	17.8
RAC30-50	38.0±1.7	42.1±4.8	11.0	SWSSRAC30-50	44.1±4.6	46.2±5.5	4.7
RAC40-50	44.8±4.0	52.9±3.0	18.0	SWSSRAC40-50	45.4±6.4	49.4±4.1	8.9
RAC50-50	55.7±6.1	57.3±6.5	2.9	SWSSRAC50-50	52.1±6.7	54.4±2.5	4.3
RAC30-100	34.3±4.1	36.6±4.7	12.5	SWSSRAC30-100	41.1±5.2	42.4±2.4	3.2
RAC40-100	42.0±2.0	43.6±5.3	3.8	SWSSRAC40-100	47.9±6.3	51.8±3.7	5.5
RAC50-100	48.0±2.9	50.7±7.0	5.6	SWSSRAC50-100	53.6±8.0	58.0±8.7	8.3

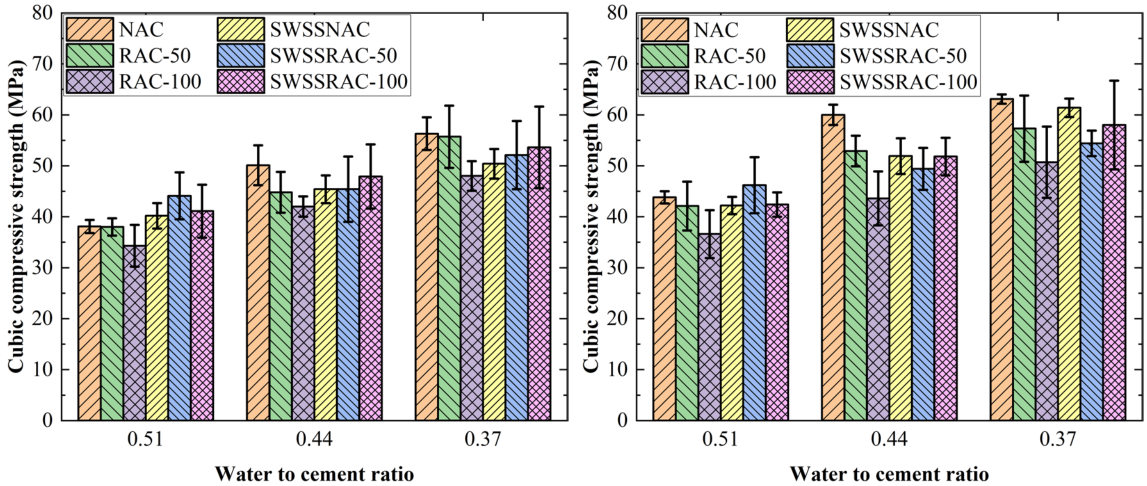

(a) 28 d (b) 180 d

Fig. 7. Experimental results of cubic compressive strength

4.3. Uniaxial compression test

4.3.1. Failure modes

Typical failure characteristics are shown in Fig. 8; the failure modes of all specimens were similar. During the test, the mortar on the surface of the ends of the specimen was constrained by the end-friction effect, and this led to lateral expansion at the middle-height section of the specimen. The shear stress during the test produces oblique cracks because of the small ultimate tensile strain of the concrete; this results in a cone at each end of the specimen. The improved effect of SW and SS on the crack resistance of RAC was greater than that of NAC. However, if the concrete was cured for a long time (180 d), the crack width of the SWSSRAC was higher than at the curing age of 28 d, because the specimen was broken into fragments at the curing age of 180 d and the specimen was still complete accompanied with some cracks (crack width around 3-5 mm) at 28 d.

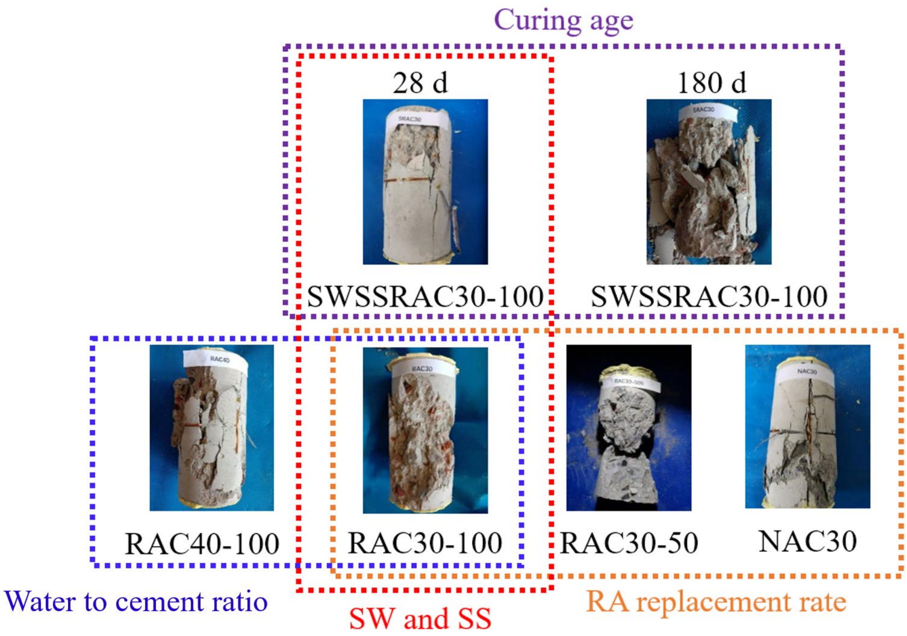

Fig. 8. Typical failure characteristics

4.3.2. Uniaxial compressive strength

The experimental results for uniaxial compressive strength are summarized in Table 6; the general trends are similar to those of cubic compressive strength. As demonstrated in Fig. 9(a), SW and SS significantly promoted the 28-day strength of concrete when the cement-to-water ratio was 0.51; the increase rate could be up to approximately 35%. In addition, the defects of the RAs were compensated after being enhanced by SW and SS, and this results in an increase in strength. For example, the 28-day strength of SWSSRAC-50 was close to that of NAC among the three types of water-to-cement ratios.

Fig. 9(b) shows that SW and SS played negative roles in the NAC especially at the low water-to-cement ratios (0.51 and 0.44). This is because the excess amount of hydration produced by the reaction between the ions in SW and cement caused a reduction in the later-age strength, especially for the NAC with a high water-to-cement ratio. However, the influence of SW and SS on the RAC still existed. The 60-day strengths of SWSSRAC30-50 and SWSSRAC30-100 were 19.3% and 23.3% higher than those of RAC30-50 and RAC30-100, respectively, when the water-to-cement ratio was 0.51. Meanwhile, the enhanced effect of SW and SS on the RAC was maintained until 180 d, as shown in Fig. 9(c). Therefore, SW and SS are not suitable for NAC but are recommended for RAC.

Table 6 Experimental results of uniaxial compressive strength

ID	Strength (MPa)			ID	Strength (MPa)		
	28 d	60 d	180 d		28 d	60 d	180 d
NAC30	29.7±1.5	31.8±2.5	31.6±0.7	SWSSNAC30	36.6±0.7	31.2±2.3	33.7±1.9
NAC40	39.6±1.1	36.9±0.6	38.5±2.0	SWSSNAC40	40.8±1.0	34.7±1.8	37.1±1.8
NAC50	44.5±1.6	42.4±2.6	42.6±2.1	SWSSNAC50	42.3±2.0	45.6±3.5	43.0±1.7
RAC30-50	29.0±3.2	31.2±1.9	29.8±4.3	SWSSRAC30-50	38.7±5.1	36.6±4.0	38.9±5.4
RAC40-50	40.0±4.2	38.4±4.3	39.3±3.8	SWSSRAC40-50	39.8±1.9	37.8±2.9	39.6±2.9
RAC50-50	42.1±4.3	46.6±3.5	46.9±2.3	SWSSRAC50-50	47.0±5.6	47.7±5.1	47.5±3.7
RAC30-100	27.9±4.1	29.9±1.7	35.4±4.4	SWSSRAC30-100	35.6±3.5	37.0±3.1	38.7±3.1
RAC40-100	38.7±3.6	34.6±1.7	37.4±1.9	SWSSRAC40-100	40.2±6.0	42.0±3.9	43.2±2.3
RAC50-100	39.8±4.4	42.3±3.9	41.1±4.6	SWSSRAC50-100	45.4±3.2	44.8±4.5	47.5±4.3

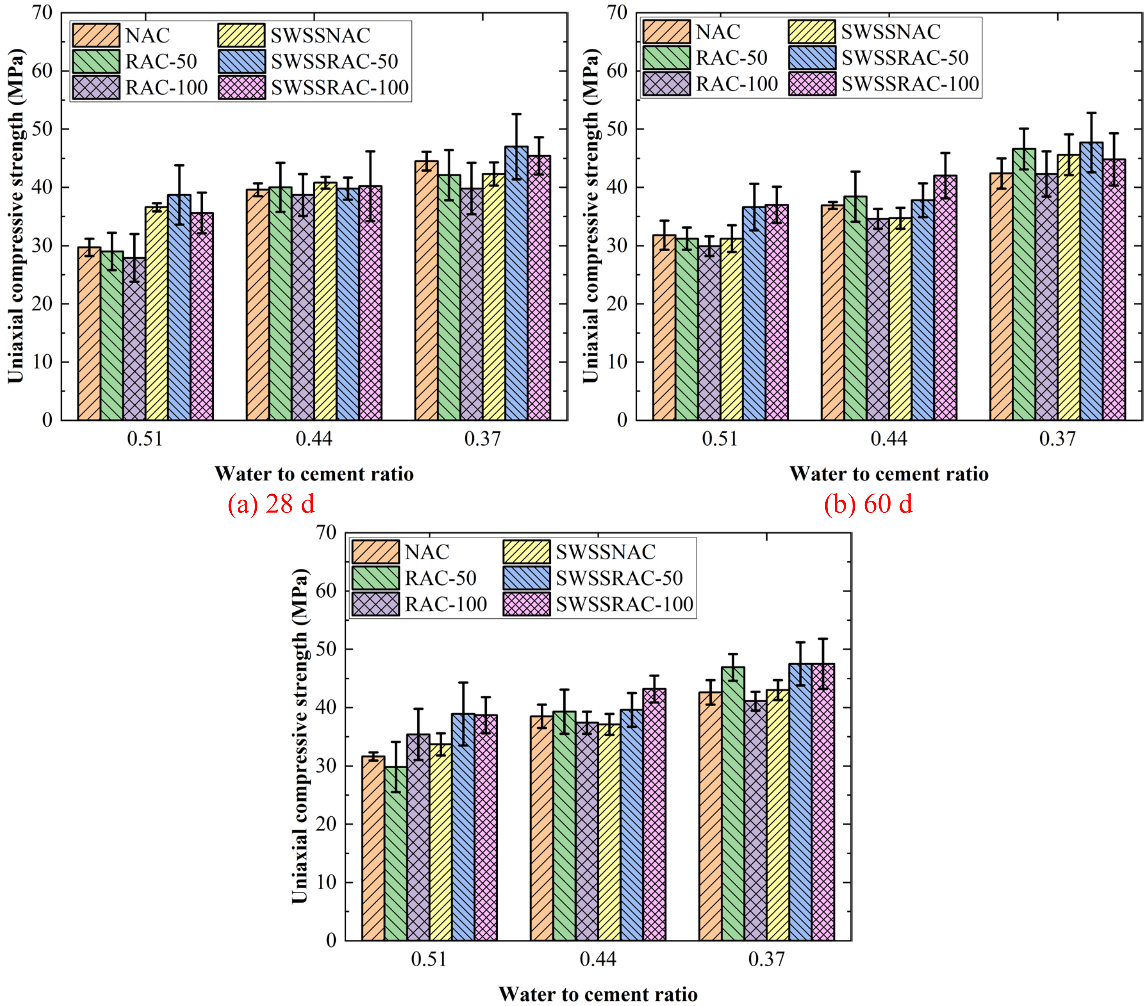

(a) 28 d (b) 60 d

(c) 180 d

Fig. 9. Experimental results of uniaxial compressive strength

4.3.3. Relationship between uniaxial and cubic compressive strength

Based on the Chinese standard GB/T 50081 [29], the ratio between the 28-day uniaxial compressive strength (f_c) and 28-day cubic compressive strength (f_{cu}) was approximately 0.79. As summarized in Table 7, the NAC ratio is consistent with the above conclusion. However, this ratio increased with the addition of SW and SS. The reason is that based on Table 8, the SW and SS increased the Poison's ratio of RAC, and the hoop effect of cubic specimen was reduced. Hence, it is necessary to establish a prediction model for the SWSSNAC and SWSSRAC. A classical model of the NAC ratio was proposed by L'Hermite [34], as shown in Eq. (1). The experimental data for SWSSNAC and SWSSRAC are plotted in Fig. 10 to further understand the effect of SW and SS on the ratio. The modified L'Hermite model (Eq. (2)) is more consistent with the test results.

Table 7 Ratio of 28-day uniaxial compressive strength to a 28-day cubic compressive strength

ID	f_c (MPa)	f_{cu} (MPa)	f_c / f_{cu}	ID	f_c (MPa)	f_{cu} (MPa)	f_c / f_{cu}
NAC30	29.7	38.1	0.78	SWSSNAC30	36.6	40.2	0.91
NAC40	39.6	50.1	0.79	SWSSNAC40	40.8	45.4	0.90
NAC50	44.5	56.3	0.79	SWSSNAC50	42.3	50.4	0.84
RAC30-50	29.0	38.0	0.76	SWSSRAC30-50	38.7	44.1	0.88
RAC40-50	40.0	44.8	0.89	SWSSRAC40-50	39.8	45.4	0.88
RAC50-50	42.1	55.7	0.76	SWSSRAC50-50	47.0	52.1	0.90
RAC30-100	27.9	34.3	0.81	SWSSRAC30-100	35.6	41.1	0.87
RAC40-100	38.7	42.0	0.92	SWSSRAC40-100	40.2	47.9	0.84
RAC50-100	39.8	48.0	0.83	SWSSRAC50-100	45.4	53.6	0.85

$$f_c = f_{cu}\left[0.76 + 0.20 \times log_{10}\left(\frac{f_{cu}}{19.6}\right)\right] \quad (1)$$

$$f_c = f_{cu}\left[0.97 - 0.26 \times log_{10}\left(\frac{f_{cu}}{19.6}\right)\right] \quad (2)$$

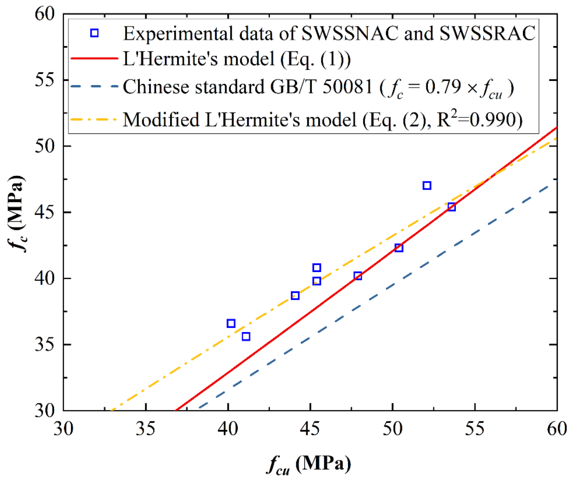

Fig. 10. Relationship between f_c and f_{cu} for SWSSNAC and SWSSRAC

4.3.4. Poisson's ratio and elastic modulus

Poisson's ratio represents the capacity of the lateral displacement of the concrete. The experimental results for Poisson's ratio are listed in Table 8. The Poisson's ratio of the NAC was approximately 0.2; the effect of curing age on the Poisson's ratio can be neglected for all mixes. In addition, the Poisson's ratio slightly decreased by around 0.02 after replacing NAs with RAs for NAC and RAC, and the influence of RA was small (±0.02) for a low water-to-cement ratio. After mixing with SW and SS, the effect of SW and SS on the Poisson's ratio of NAC was less than that of RAC, and the improved effect on RAC reached 20% on average.

Table 8 Experimental results of Poisson's ratio

ID	Poisson's ratio			ID	Poisson's ratio		
	28 d	60 d	180 d		28 d	60 d	180 d
NAC30	0.19±0.007	0.21±0.007	0.20±0.006	SWSSNAC30	0.16±0.004	0.16±0.003	0.18±0.004
NAC40	0.20±0.008	0.21±0.007	0.21±0.002	SWSSNAC40	0.17±0.005	0.19±0.008	0.18±0.004
NAC50	0.22±0.009	0.22±0.007	0.22±0.007	SWSSNAC50	0.21±0.007	0.20±0.010	0.19±0.009
RAC30-50	0.16±0.012	0.17±0.011	0.17±0.008	SWSSRAC30-50	0.18±0.015	0.18±0.006	0.20±0.020
RAC40-50	0.19±0.017	0.18±0.014	0.19±0.007	SWSSRAC40-50	0.20±0.011	0.23±0.027	0.22±0.009
RAC50-50	0.22±0.026	0.23±0.011	0.20±0.024	SWSSRAC50-50	0.20±0.023	0.23±0.022	0.23±0.018
RAC30-100	0.18±0.014	0.19±0.021	0.18±0.017	SWSSRAC30-100	0.17±0.005	0.19±0.021	0.19±0.012
RAC40-100	0.18±0.021	0.20±0.021	0.18±0.012	SWSSRAC40-100	0.21±0.007	0.20±0.021	0.21±0.008
RAC50-100	0.21±0.023	0.21±0.015	0.20±0.017	SWSSRAC50-100	0.23±0.015	0.22±0.008	0.22±0.015

The experimental results for the elastic modulus are summarized in Table 9. The growth rate of the elastic modulus of each group can be neglected (less than 5%) when the curing age of NAC or RAC is greater than 60 d. For SWSSNAC, the elastic modulus at 180 d was approximately 15% lower than that at 28 d, showing that SW and SS had an obvious weakening effect on the rigidity of the NAC. However, the weakening effect of the SW and SS on the elastic modulus was reduced to less than 5% with an increase in the RA replacement rate. As shown in Fig. 11(a), the elastic modulus decreases with an increase in the replacement rate of RA because the interface transition zone of the RAC is weak due to the old mortar wrapped on the surface of the RAs; this reduces the rigidity of the specimen. Further, SW and SS can increase the 28-day elastic moduli of the NAC and RAC. Fig. 11(b) shows that the concrete specimens mixed with SW and SS were almost equal to those without SW and SS for the same mix proportion. Meanwhile, the elastic modulus still decreased with an increase in the replacement rate of RA. In other words, the influence of the RA replacement rate on the elastic modulus was greater than that of the SW and SS. Fig. 11(c) shows that impurities in SW and SS reduced the elastic modulus with an increase in the curing age, compared with the elastic modulus measured at 28 d.

Table 9 Experimental results of elastic modulus

ID	Elastic modulus (GPa)			ID	Elastic modulus (GPa)		
	28 d	60 d	180 d		28 d	60 d	180 d
NAC30	25.9±1.1	28.6±1.2	28.5±1.1	SWSSNAC30	29.8±1.4	28.5±1.0	23.0±0.9
NAC40	30.3±0.9	31.7±0.3	31.4±0.5	SWSSNAC40	33.2±0.7	31.9±0.7	27.8±1.0
NAC50	32.1±0.8	38.1±1.0	38.4±0.8	SWSSNAC50	34.2±1.0	36.1±1.0	33.0±1.7
RAC30-50	23.7±2.1	27.3±3.2	27.3±2.6	SWSSRAC30-50	28.0±1.7	28.4±1.3	27.7±2.5
RAC40-50	28.3±1.3	28.2±1.4	30.1±2.7	SWSSRAC40-50	32.4±2.3	29.5±3.4	27.5±2.1
RAC50-50	30.9±1.5	34.7±4.0	35.8±3.0	SWSSRAC50-50	31.1±1.9	31.8±2.0	32.3±1.5
RAC30-100	21.0±2.4	23.8±0.8	24.6±2.3	SWSSRAC30-100	24.9±2.0	23.6±1.8	23.0±2.1
RAC40-100	22.5±2.4	24.4±2.7	24.4±0.9	SWSSRAC40-100	26.9±1.8	28.0±2.4	28.5±1.5
RAC50-100	25.6±3.0	27.6±3.1	25.5±2.3	SWSSRAC50-100	31.8±3.7	29.7±2.8	29.7±1.7

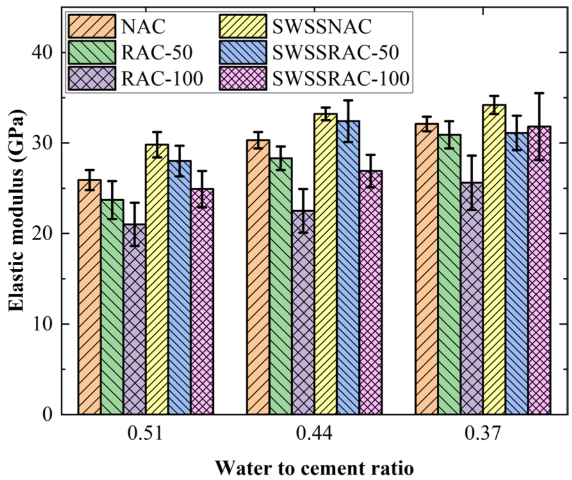

(a) 28 d

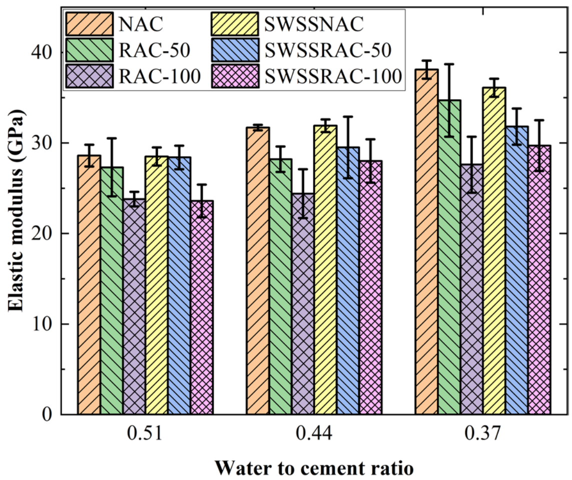

(b) 60 d

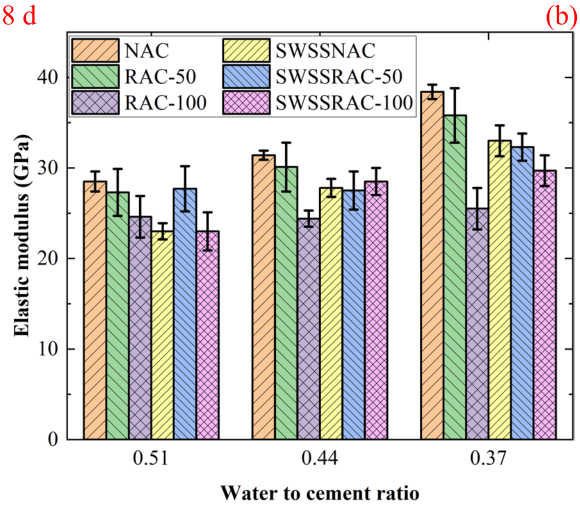

(c) 180 d

Fig. 11. Relationship between elastic modulus and water-to-cement ratio

In the Chinese code, the relationship between the 28-day elastic modulus (E_c) and 28-day cubic compressive strength (f_{cu}) can be described as:

$$E_c = \frac{100}{p+\frac{q}{f_{cu}}}, \tag{3}$$

where p and q represent the undetermined parameters. For the NAC, according to the Chinese code [35], p and q are equal to 2.2 and 34.7, respectively. For RAC, Xiao et al. [36] proposed that p and q should be modified to 2.6 and 42.2, respectively. The relationship between the elastic modulus and uniaxial compressive strength is discussed because the elastic properties correspond to uniaxial stress. The 28-day cubic compressive strength in the existing models was converted to the 28-day uniaxial compressive strength based on the discussion in Subsection 4.3.3. Fig. 12 shows the experimental data of RAC in this investigation are consistent with the modified model proposed by Xiao et al. [36]; this is also consistent with other RAC test results (Zhao et al. [37]; Carnerio et al. [38]). However, considering the influence of adding SW and SS on the elastic modulus of RAC, a proposed model for SWSSRAC, based on Eq. (3) is proposed as:

$$E_c = \frac{100}{1+\frac{100}{f_c}} \tag{4}$$

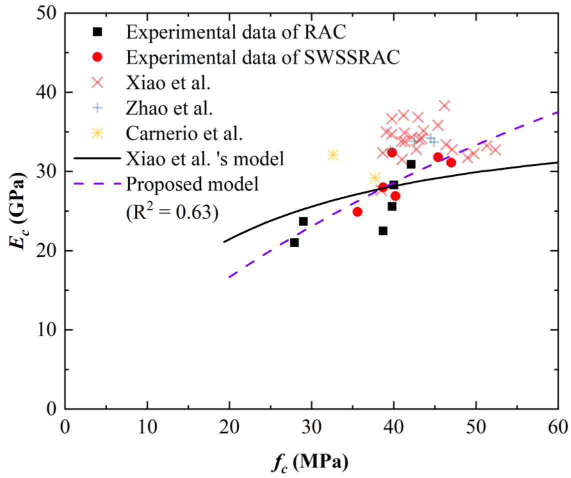

Fig. 12. Relationship between elastic modulus and uniaxial compressive strength

4.3.5. Stress–strain relationship

Typical stress–strain curves are plotted in Fig. 13. The specimen began to accumulate irreparable damage when the compressive load reached approximately 40% of the peak load with a gradual increase in stress [31]; the curve increased nonlinearly. In other words, the specimens entered the plastic deformation stage. The curve forms a single peak with a slope equal to zero and begins to enter the descending section when the peak point is reached. Subsequently, the downward trend was nonlinear because of the continuous occurrence of new cracks in the descending section of the curve.

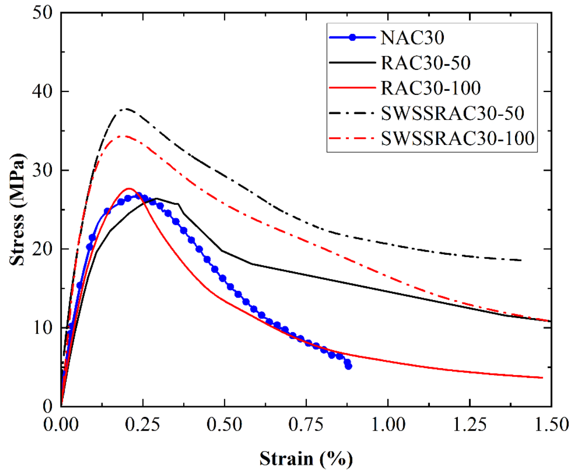

Fig. 13. Relationship between stress and strain at the 28 d curing age

By observing the area bounded by the strain axis from the peak stress to the 80% peak stress, the slowing rate near the peak stress of RAC was around 25% higher than that of the NAC because of the defects in the RAs. However, after utilizing RAs, the displacement capacity was enhanced because of the large number of cracks and pores in RAC; the RAC specimens failed later than NAC. In other words, the ultimate strain of NAC was much smaller than that of RAC and SWSSRAC. Fig. 14(a) shows the long-term stress–strain relationship between the NAC and RAC is close in both the ascending and descending segments. However, the descending segments of the curve of SWSSRAC are obviously shortened at the 180-day curing age after mixing SW and SS, as shown in Fig. 14(b). The brittleness of the SWSSRAC increased with an increase in the curing age because the salt generated by SW and SS during the hydration reaction of cement fills the pores with the slurry and old mortar on the RAs, which forms a stronger structure and smaller deformation capacity for the SWSSRAC. It is necessary to use other enhanced methods (such as fibers) to strengthen the toughness of SWSSRAC if applied in seismic areas because of the short displacement capacity for safety [39], especially for SWSSRAC with a 100% RA replacement rate.

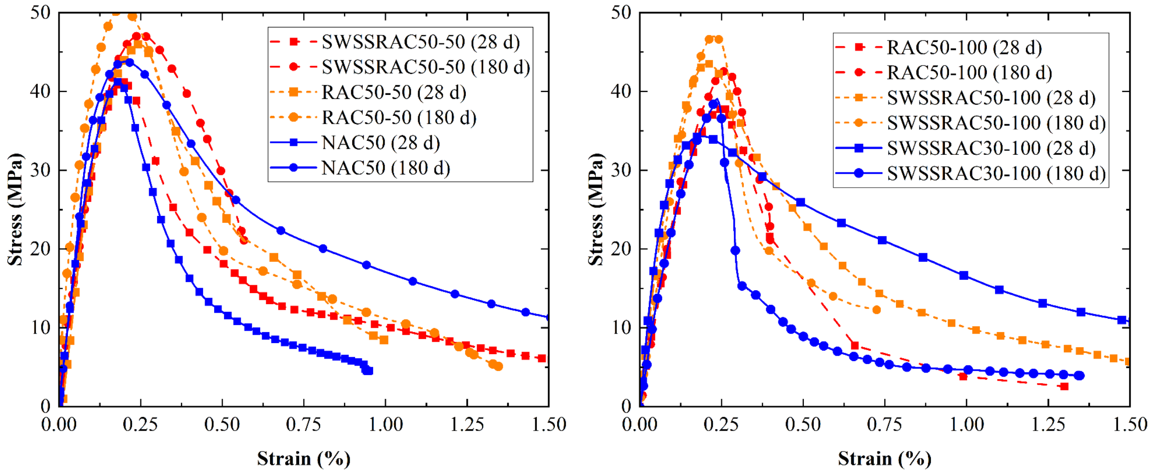

(a) (b)

Fig. 14. Influence of curing age on the stress-strain curve from 28 d to 180 d

5. Discussions of the constitutive model for SWSSRAC

5.1. Review of the constitutive models for RAC

The constitutive model of ordinary concrete (NAC) has been studied by many researchers. The model proposed by Guo [40] is a commonly used model, which is given as:

$$y = ax + (3-2a)x^2 + (a-2)x^3 \ \ (x \leq 1)$$
$$y = \frac{x}{b(x-1)^2 + x} \ (x > 1) \tag{5}$$

where y represents the ratio of the stress data to the peak stress ($y = \sigma/f_c$), x represents the ratio of the strain data to the strain corresponding to the peak stress ($x = \varepsilon/\varepsilon_c$), and a and b represent the shape parameters.

However, by conducting several experiments for the RAC because of the defects of RAs, Xiao et al. [41] found that the shaped parameters obey:

$$a = 2.2(0.748r^2 - 1.231r + 0.975)$$
$$b = 0.8(7.648r + 1.142) \tag{6}$$

where r represents the RA replacement percentage. Recently, Huang et al. [42] further considered the effect of chloride ion content of SS (φ) on RAC incorporated with SS (SSRAC) at the curing age of 28 d based on the model proposed by Xiao et al. [41], as shown by:

$$a = 2.25[(-0.046 + 0.962 \times 10^5\varphi^2)r^2 - (0.11 + 74\varphi)r] - 120\varphi + 0.955$$
$$b = 2.3(0.12 - 71.7\varphi)r + 174.8\varphi + 1.043 \tag{7}$$

However, there have been few studies on the constitutive model of SWSSRAC, and it is necessary to further discuss the experimental data in this investigation.

5.2. Relationship between the peak stress and peak strain

The variables *x* and *y* in the constitutive model are related to the relationship and therefore, it is necessary to understand the relationship between the peak stress (f_c) and its corresponding strain (peak strain, ε_c) before analyzing the constitutive model of SWSSRAC. Based on Xiao et al.'s [41] result, the relationship can be described as:

$$f_c = 1.84\varepsilon_c + 10.32 \tag{7}$$

where the units of f_c and ε_c are MPa and 10^{-2}, respectively. Fig. 15 shows that the experimental data for SWSSRAC are consistent with those of Xiao et al. [41] (RMSE = 0.000229). The use of SW and SS had no effect on the relationship between the peak strain and peak stress of the RAC.

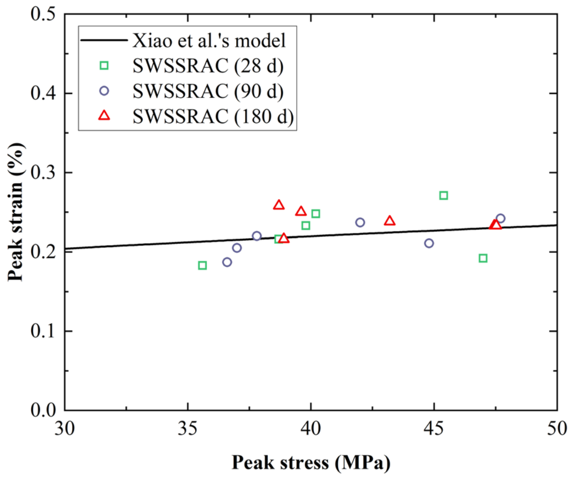

Fig. 15. Relationship between the peak stain and peak stress for SWSSRAC

5.3. Comparison between the experimental data and existing models

The experimental data of the SWSSRAC were compared with the existing models, as shown in Fig. 16, where chloride ion content of SS $\varphi = 0.082\%$ was utilized based on the mix proportion in this investigation. Compared with the model proposed by Xiao et al. [41] and Huang et al. [42], the reduction rate of the falling segment of RAC can be enhanced by increasing the chloride ion content. Fig. 16(a) shows that the chlorinity was high after utilizing SW and SS in RAC mixes; however, the experimental data generally satisfied Huang et al.'s model [42]. The difference is caused by many cracks during the unloading phase of the specimen and the deviation of the measurement caused by the looseness of the LVDTs.

However, as shown in Fig. 16(b), the phenomenon was different when the RA replacement rate was 100%. The experimental data at 28 d were consistent with Huang et al.'s model [42]. If the curing age is 180 d, the toughening effect of SW and SS can be neglected when analyzing the constitutive model, i.e. the experimental data at 180 d is close to the model proposed by Xiao et al. [41] for RAC. Recently, SWSSRAC was also tested by Xiao et al. and published in another literature [43], where the RA replacement rate was 100% and the compressive strength is around 40 MPa at the curing age of 28 d. As shown in Fig. 17, compared with Xiao et al.'s model [41], Xiao et al.'s results on SWSSRAC [43] are closer to Huang et al.'s model [42]. Specifically, the RMSE of Huang et al.'s model [42] is 50% smaller than that of Xiao et al.'s model [41]. In conclusion, Huang et al.'s model [42] can be considered applicable to SWSSRAC at a curing age of 28 d. However, it is necessary to use Xiao et al.'s model [41] for SWSSRAC when long-term use needs to be considered and a high replacement rate of RA is designed for safety reasons.

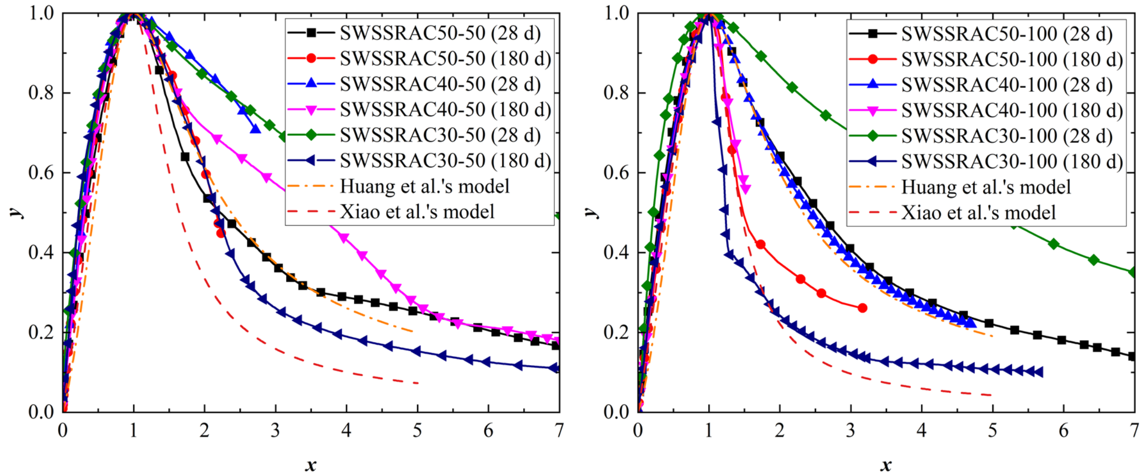

Fig. 16. Comparison between the experimental data and existing models

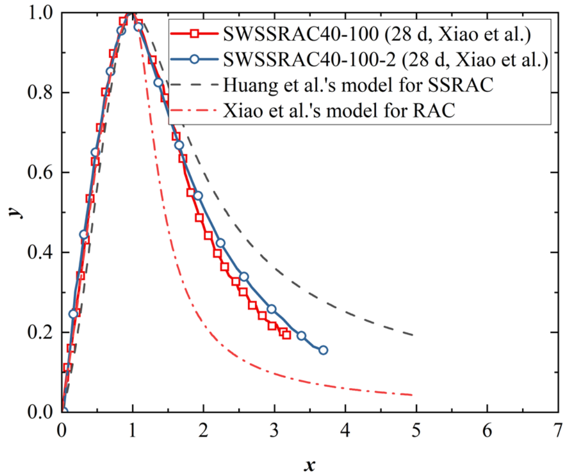

Fig. 17. Comparison between the existing models and data in other literatures

6. Conclusions

RAC with SW and SS is conducive to sustainable green development and plays a positive role in the recycling of C&D waste in the future. In this study, the working performance and compressive behaviors of SWSSRAC were studied; the constitutive model was also studied. The conclusions are as follows:

(1) The fluidity of SWSSRAC was slightly worse than that of RAC under the same water-to-cement ratio; the effect of the RA replacement rate on the fluidity of concrete was greater than that of mixing with SW and SS.

(2) The compressive strength of SWSSRAC at 28 d is higher than that of NAC and RAC. In terms of the long curing age (180 d), the strength of SWSSRAC with the same water-to-cement ratio was higher than that of RAC; however, it is lower than that of NAC.

(3) The ratio of the cubic compressive strength to the uniaxial compressive strength of concrete can be enhanced using SW and SS in concrete mixes. Therefore, a model for the SWSSRAC ratio was proposed based on the classical model for NAC. Further, the influence of the RA replacement rate on the elastic modulus was greater than that of the SW and SS. A prediction model for the elastic modulus of SWSSRAC was proposed based on the model for RAC.

(4) For the stress–strain relationship, the deformation capacity of SWSSRAC decreases

with an increase in the curing age. This is because the salt generated by SW and SS during the hydration reaction of cement fills the pores with the slurry and old mortar on the RAs, which forms a stronger structure and smaller deformation capacity for the SWSSRAC.

(5) After reviewing the existing models of RAC, it was found that Huang et al.'s model [42] can be applicable to SWSSRAC at a curing age of 28 d. However, a high replacement rate of RA is designed when long-term use needs to be considered for safety reasons, and it is necessary to use Xiao et al.'s model [41] for SWSSRAC.

Above all, SW and SS are more suitable for RAC than NAC, and SWSSRAC is a sustainable material that can be used in coastal structures with FRP reinforcement. The mechanism of the effect of SW and SS on the RAC under various curing ages will be further explored on the microstructure scale.

Acknowledgements

This study was funded by the Guangdong Basic and Applied Basic Research Foundation (2022A1515010008), Natural Science Foundation of Guangxi Province (2021GXNSFAA220045, 2021GXNSFBA075014), China Postdoctoral Science Foundation (2021M690765), Systematic Project of Guangxi Key Laboratory of Disaster Prevention and Engineering Safety (2021ZDK007), National Natural Science Foundation of China (52108199), Guangxi Science and Technology Department (AD21238007), and the Science and Technology Planning Project of Guangzhou (202102080269, 202201011086).

References

[1] W. Feng, Z. Chen, Y. Tang, F. Liu, F. Yang, Y. Yang, B.A. Tayeh, A. Namdar, Fracture characteristics of sustainable crumb rubber concrete under a wide range of loading rates, Constr. Build. Mater. 359 (2022) 129474. https://doi.org/10.1016/j.conbuildmat.2022.129474.

[2] W.H. Feng, Y.C. Tang, W.M. He, W.B. Wei, Y.M. Yang, Mode I dynamic fracture toughness of rubberised concrete using a drop hammer device and split Hopkinson pressure bar, J. Build. Eng. 48 (2022) 103995. https://doi.org/10.1016/j.jobe.2022.103995.

[3] Y.C. Tang, W.H. Feng, Z. Chen, Y.M. Nong, S.H. Guan, J.B. Sun, Fracture behavior of a

sustainable material: Recycled concrete with waste crumb rubber subjected to elevated temperatures, J. Clean. Prod. 318 (2021) 128553. https://doi.org/10.1016/j.jclepro.2021.128553.
[4] W. Feng, Y. Wang, J. Sun, Y. Tang, D. Wu, Z. Jiang, J. Wang, X. Wang, Prediction of thermo-mechanical properties of rubber-modified recycled aggregate concrete, Constr. Build. Mater. 318 (2022) 125970. https://doi.org/10.1016/j.conbuildmat.2021.125970.
[5] J. Zhang, L. Ding, F. Li, J. Peng, Recycled aggregates from construction and demolition wastes as alternative filling materials for highway subgrades in China, J. Clean. Prod. 255 (2020) 120223. https://doi.org/10.1016/j.jclepro.2020.120223.
[6] H. Naderpour, M. Mirrashid, Estimating the compressive strength of eco-friendly concrete incorporating recycled coarse aggregate using neuro-fuzzy approach, J. Clean. Prod. 265 (2020) 121886. https://doi.org/10.1016/j.jclepro.2020.121886.
[7] Y.C. Tang, L.J. Li, C.L. Wang, M.Y. Chen, W.X. Feng, X.J. Zou, K.Y. Huang, Real-time detection of surface deformation and strain in recycled aggregate concrete-filled steel tubular columns via four-ocular vision, Robot. Comput.-Integr. Manuf. 59 (2019) 36–46. https://doi.org/10.1016/j.rcim.2019.03.001.
[8] Y. Tang, Z. Huang, Z. Chen, M. Chen, H. Zhou, H. Zhang, J. Sun, Novel visual crack width measurement based on backbone double-scale features for improved detection automation, Eng. Struct. 274 (2023) 115158. https://doi.org/10.1016/j.engstruct.2022.115158.
[9] Z. Xiong, Q.L. Cai, F. Liu, L.J. Li, Y.L. Long, Dynamic performance of RAC-filled double-skin tubular columns subjected to cyclic axial compression, Constr. Build. Mater. 248 (2020) 118665. https://doi.org/10.1016/j.conbuildmat.2020.118665.
[10] D. Pan, S.A. Yaseen, K. Chen, D. Niu, C.K. Ying Leung, Z. Li, Study of the influence of seawater and sea sand on the mechanical and microstructural properties of concrete, J. Build. Eng. 42 (2021) 103006. https://doi.org/10.1016/j.jobe.2021.103006.
[11] J.G. Teng, Y. Xiang, T. Yu, Z. Fang, Development and mechanical behaviour of ultra-high-performance seawater sea-sand concrete, Adv. Struct. Eng. 22 (2019) 3100–3120. https://doi.org/10.1177/1369433219858291.
[12] F.M. Wegian, Effect of seawater for mixing and curing on structural concrete, IES J. Part Civ. Struct. Eng. 3 (2010) 235–243. https://doi.org/10.1080/19373260.2010.521048.
[13] Q. Li, H. Geng, Y. Huang, Z. Shui, Chloride resistance of concrete with metakaolin addition and seawater mixing: A comparative study, Constr. Build. Mater. 101 (2015) 184–192. https://doi.org/10.1016/j.conbuildmat.2015.10.076.
[14] M. Islam, S. Islam, A. Amin, M. Islam, Sustability of sea water on curing and compressive strength of structural concrete, J. Civ. Eng. IEB. 40 (2012) 37–45.
[15] U.G. Eziefula, J.C. Ezeh, B.I. Eziefula, Properties of seashell aggregate concrete: A review, Constr. Build. Mater. 192 (2018) 287–300. https://doi.org/10.1016/j.conbuildmat.2018.10.096.
[16] E.-I. Yang, S.-T. Yi, Y.-M. Leem, Effect of oyster shell substituted for fine aggregate on concrete characteristics: Part I. Fundamental properties, Cem. Concr. Res. 35 (2005) 2175–2182. https://doi.org/10.1016/j.cemconres.2005.03.016.

[17] J. Limeira, M. Etxeberria, L. Agulló, D. Molina, Mechanical and durability properties of concrete made with dredged marine sand, Constr. Build. Mater. 25 (2011) 4165–4174. https://doi.org/10.1016/j.conbuildmat.2011.04.053.
[18] M. Cui, J.Z. Mao, D.G. Jia, B. Li, Experimental study on mechanical properties of marine sand and seawater concrete, in: Atlantis Press, Wuhan, China, 2014: pp. 106–111. https://doi.org/10.2991/icmce-14.2014.19.
[19] L.B. Bian, S.M. Song, F. Li, Research on durability of concrete with sea sand, China Concr. Cem. Prod. (2012) 11–14. https://doi.org/10.3969/j.issn.1000-4637.2012.02.003.
[20] K. Karthikeyan, V. Nagarajan, Feasibility study on utilization of marine sand in concrete for sustainable development, Indian J. Geo Mar. Sci. 45 (2016) 313–318.
[21] M.B. Leite, P.J.M. Monteiro, Microstructural analysis of recycled concrete using X-ray microtomography, Cem. Concr. Res. 81 (2016) 38–48. https://doi.org/10.1016/j.cemconres.2015.11.010.
[22] S. Pradhan, S. Kumar, S.V. Barai, Multi-scale characterisation of recycled aggregate concrete and prediction of its performance, Cem. Concr. Compos. 106 (2020) 103480. https://doi.org/10.1016/j.cemconcomp.2019.103480.
[23] E.A.B. Koenders, M. Pepe, E. Martinelli, Compressive strength and hydration processes of concrete with recycled aggregates, Cem. Concr. Res. 56 (2014) 203–212. https://doi.org/10.1016/j.cemconres.2013.11.012.
[24] M. Etxeberria, E. Vázquez, A. Marí, M. Barra, Influence of amount of recycled coarse aggregates and production process on properties of recycled aggregate concrete, Cem. Concr. Res. 37 (2007) 735–742. https://doi.org/10.1016/j.cemconres.2007.02.002.
[25] C. Alexandridou, G.N. Angelopoulos, F.A. Coutelieris, Mechanical and durability performance of concrete produced with recycled aggregates from Greek construction and demolition waste plants, J. Clean. Prod. 176 (2018) 745–757. https://doi.org/10.1016/j.jclepro.2017.12.081.
[26] ASTM-International, ASTM D1141: Standard practice for the preparation of substitute ocean water, 2013.
[27] Chinese standard, JGJ 52: Standard for technical requirements and test method of sand and crushed stone (or gravel) for ordinary concrete, 2006.
[28] Chinese standard, JGJ 55: Specification for mix proportion design of ordinary concrete, 2011.
[29] Chinese standard, GB/T 50081: Standard for test methods of concrete physical and mechanical properties, 2019.
[30] ASTM-International, ASTM C39: Standard test method for compressive strength of cylindrical concrete specimens, 2020.
[31] ASTM-International, ASTM C469: Standard test method for static modulus of elasticity and Poisson's ratio of concrete in compression, 2014.
[32] J. Liu, R. An, Z. Jiang, H. Jin, J. Zhu, W. Liu, Z. Huang, F. Xing, J. Liu, X. Fan, T. Sui, Effects of w/b ratio, fly ash, limestone calcined clay, seawater and sea-sand on workability, mechanical properties, drying shrinkage behavior and micro-structural characteristics of concrete, Constr. Build. Mater. 321 (2022) 126333.

https://doi.org/10.1016/j.conbuildmat.2022.126333.
[33] M.Z.Y. Ting, K.S. Wong, M.E. Rahman, M. Selowara Joo, Mechanical and durability performance of marine sand and seawater concrete incorporating silicomanganese slag as coarse aggregate, Constr. Build. Mater. 254 (2020) 119195. https://doi.org/10.1016/j.conbuildmat.2020.119195.
[34] R. L'Hermite, La Documentation technique du batiment et des travaux publics, Idées actuelles sur la technologie du béton, Paris, France, 1955.
[35] Chinese standard, GB/T 50080: Standard for test method of performance on ordinary fresh concrete, 2016.
[36] J. Xiao, K. Zhang, A. Akbarnezhad, Variability of stress-strain relationship for recycled aggregate concrete under uniaxial compression loading, J. Clean. Prod. 181 (2018) 753–771. https://doi.org/10.1016/j.jclepro.2018.01.247.
[37] J.L. Zhao, T. Yu, J.G. Teng, Stress-strain behavior of FRP-confined recycled aggregate concrete, J. Compos. Constr. 19 (2015) 04014054. https://doi.org/10.1061/(ASCE)CC.1943-5614.0000513.
[38] J.A. Carneiro, P.R.L. Lima, M.B. Leite, R.D. Toledo Filho, Compressive stress–strain behavior of steel fiber reinforced-recycled aggregate concrete, Cem. Concr. Compos. 46 (2014) 65–72. https://doi.org/10.1016/j.cemconcomp.2013.11.006.
[39] J.-J. Zeng, J. Liao, Y. Zhuge, Y.-C. Guo, J.-K. Zhou, Z.-H. Huang, L. Zhang, Bond behavior between GFRP bars and seawater sea-sand fiber-reinforced ultra-high strength concrete, Eng. Struct. 254 (2022) 113787. https://doi.org/10.1016/j.engstruct.2021.113787.
[40] Z.H. Guo, The strength and deformation of concrete-experimental results and constitutive relationship, Tsinghua University Press, Beijing, 1999.
[41] J. Xiao, J. Li, Ch. Zhang, Mechanical properties of recycled aggregate concrete under uniaxial loading, Cem. Concr. Res. 35 (2005) 1187–1194. https://doi.org/10.1016/j.cemconres.2004.09.020.
[42] Y. Huang, X. He, Q. Wang, Y. Sun, Mechanical properties of sea sand recycled aggregate concrete under axial compression, Constr. Build. Mater. 175 (2018) 55–63. https://doi.org/10.1016/j.conbuildmat.2018.04.136.
[43] J. Xiao, K. Zhang, Q. Zhang, Strain rate effect on compressive stress–strain curves of recycled aggregate concrete with seawater and sea sand, Constr. Build. Mater. 300 (2021) 124014. https://doi.org/10.1016/j.conbuildmat.2021.124014.